Coupled-channels calculations of elastic and inelastic scattering

H. Esbensen and F. Videbaek
Physics Division, Argonne National Laboratory, Argonne, Illinois 60439
(Received 24 February 1989)

Cross sections for the elastic and inelastic scattering of ^{16}O on ^{58}Ni, ^{88}Sr, ^{40}Ca, and ^{48}Ca have been calculated in a coupled-channels treatment, including the low-lying 2^+ and 3^- states of both projectile and target. Real, energy-independent ion-ion potentials and form factors were used, and fusion was simulated by ingoing wave boundary conditions in all channels. The agreement with the measured scattering data is qualitatively as good as obtained in previous optical-model calculations.

I. INTRODUCTION

In recent years it has been realized that the optical potential extracted from fitting elastic scattering data in the distorted-wave Born approximation (DWBA) can have a strong energy dependence near the Coulomb barrier. This has been demonstrated for the reactions ^{16}O+^{208}Pb (Ref. 1) and ^{16}O+^{60}Ni.[2] The energy dependence has been explained from a dispersion relation between the real and the imaginary part of the optical potential and the fact that the effect of nuclear couplings diminishes as the energy is decreased below the Coulomb barrier.[3]

A physically more satisfying approach is to perform explicit coupled-channels calculations which include the most dominant reaction channels. In this approach one uses a real, energy-independent ion-ion potential, whereas the energy-dependent polarization potential is generated implicitly from the couplings. We have calculated the cross sections for elastic and inelastic scattering of ^{16}O on ^{58}Ni, ^{88}Sr, ^{40}Ca, and ^{48}Ca, and made detailed comparisons to measurements.[4,5] Previous analyses have been based on optical-model calculations. We have used a coupled-channels treatment and included the inelastic 2^+ and 3^- excitations of both projectile and target. The calculations are based on a real, energy-independent ion-ion potential, which has been determined empirically.[6]

The one- and two-nucleon transfer channels are suppressed at energies near the Coulomb barrier due to unfavorably large negative Q values in most of the reactions we have studied. The magnitude of the one-proton cross section is 1–20 mb for ^{58}Ni (Ref. 7) and ^{88}Sr,[8] and it is smaller than the cross section for inelastic excitations. We shall ignore the transfer channels in our calculations. They may become important at the highest energies that we have considered. Transfer channels can play an important role for other systems near Coulomb barrier. An example is the ^{16}O+^{208}Pb scattering, which previously has been studied in a coupled-channels treatment.[9,10]

II. THE ION-ION POTENTIAL AND FORM FACTORS

The empirical ion-ion potential that we have used has been extracted from an overall fit to the elastic scattering data of several light and intermediate heavy projectile-target combinations.[6] We have used a Wood-Saxon parametrization, which is adjusted to fit the tail of the empirical potential,

$$U_N(r)=-31.67\ \text{MeV fm}^{-1}\frac{R_1R_2}{R_1+R_2}\{1+\exp[(r-R_1-R_2-DR)/a]\}^{-1},$$

where $R_i=1.233A_i^{1/3}-0.98A_i^{-1/3}$ fm, $DR=0.29$ fm, and $a=0.63$ fm.

Elastic scattering data for ^{16}O on ^{48}Ca, ^{58}Ni, and ^{88}Sr were included in the determination of the parameters for the ion-ion potential,[6] whereas no data for ^{16}O+^{40}Ca were considered. We have found it necessary to make a slight adjustment of DR for the latter system in order to improve the fits and have chosen $DR=0.44$ fm. This adjustment is equivalent to a slightly larger radius for ^{40}Ca than predicted by the above formula (from 3.93 to 4.08 fm). It is interesting to note that with this adjustment the ratio of the radii for ^{40}Ca and ^{48}Ca are now consistent with the ratio of the measured matter rms radii.[11]

We solve the conventional coupled equations for inelastic scattering. The radial wave functions for the inelastic channels are generated by a direct coupling to the elastic channel

$$\left\{\frac{\hbar^2}{2\mu}\left[-\frac{d^2}{dr^2}+\frac{l_\beta(l_\beta+1)}{r^2}\right]+\frac{Z_1Z_2e^2}{r}+U_N(r)+E_x-E_{\text{c.m.}}\right\}u^l_{l_\beta\lambda}(r)=-[F^\lambda_C(r)+F^\lambda_N(r)](-1)^\lambda\langle l0\lambda0|l_\beta0\rangle u^l_{l0}(r),$$

where the Coulomb and nuclear form factors are

$$F^\lambda_C(r)=\frac{(\beta R)_C}{\sqrt{4\pi}}\frac{3R_C^{\lambda-1}}{2\lambda+1}\frac{Z_1Z_2e^2}{r^{\lambda+1}},$$

$$F_N^{\lambda}(r)=-\frac{(\beta R)_N}{\sqrt{4\pi}}\frac{\partial U_N(r)}{\partial r}\ .$$

Above, the total angular momentum is denoted by l, and it is identical to the orbital angular momentum in the elastic channel. The orbital angular momenta in the inelastic channels are denoted by l_β, and they can assume all values that can be reached by the coupling of the multipolarity λ of the excitation to the total angular momentum l. The radial wave function for the elastic channel is similarly determined by couplings to all included inelastic channels,

$$\left\{\frac{\hbar^2}{2\mu}\left[-\frac{d^2}{dr^2}+\frac{l(l+1)}{r^2}\right]+\frac{Z_1Z_2e^2}{r}+U_N(r)-E_{\text{c.m.}}\right\}u_{l0}^{l}(r)=-\sum_{\lambda l_\beta}[F_C^{\lambda}(r)+F_N^{\lambda}(r)](-1)^{\lambda}\langle l0\lambda0|l_\beta0\rangle u_{l_\beta}^{l}\lambda(r)\ .$$

The spectroscopic input for the various reaction calculations is given in Table I. The $B(E\lambda)$ values for the Coulomb coupling are taken from the literature (Refs. 12 and 14–17). The nuclear coupling strengths depend on the parametrization of the ion-ion (or optical) potential used to analyze the data. The strengths given in Table I are the values we have obtained to give a reasonable fit to the data. For the oxygen states, however, we have used the values determined in Ref. 13 from alpha scattering. The values obtained in Refs. 4 and 5 are shown for comparison in the last column of Table I.

We solve the coupled equations with the usual scattering boundary conditions at large separations. At small distances, inside the Coulomb barrier, we impose ingoing wave boundary conditions in all channels to simulate the fusion process. The exact location turns out to be not so important, but the distance of maximum nuclear attraction, $r=R_1+R_2+DR$, is a reasonable choice.

III. ^{16}O+^{58}Ni AND ^{16}O+^{88}Sr SCATTERING

The energy dependence of the cross sections for elastic and inelastic 2^+ scattering have been measured systematically for the reactions ^{16}O+^{58}Ni and ^{16}O+^{88}Sr.[4] A comparison of our calculations to the measured angular distributions for ^{16}O+^{58}Ni is shown in Fig. 1. The fully drawn curves are the results of including all the 2^+ and 3^- states given in Table I, for both projectile and target. The nuclear coupling strength of the 2^+ state in the target has been adjusted to make a reasonable fit to the data. The dashed curves were obtained by including the 2^+ state in ^{58}Ni as the only inelastic channel. The couplings to the other inelastic channels are seen to have a significant effect on both the elastic scattering and the inelastic 2^+ excitation. The most obvious discrepancy appears at 44 MeV, where the elastic scattering data are about 20% higher than the full calculation at large scattering angles.

The calculated 2^+ cross sections at 60 MeV deviate also significantly from the data at large scattering angles. In particular, the calculated angular distribution contains an interference pattern with a period of about 6°–8°. This reflects the presence of a strong and narrow peak in the 2^+ S matrix as a function of the orbital angular momentum near $l=25$, which is slightly below the grazing l value of 28. The same pattern also appears in the elastic scattering calculation.

The energy dependence of the differential cross sections is illustrated in Fig. 2 at different fixed scattering angles. The agreement is very good for elastic scattering at 175°. The elastic scattering data at 60°–90° are generally 20–30% larger than the calculated cross section at the 10% level of Rutherford scattering. This may partly be due to systematic errors in the measurements. In fact, the angular distributions measured at fixed beam energy (shown in Fig. 1) have an overlap with the data shown in

TABLE I. Spectroscopic input to the calculations. The nuclear coupling strengths marked by an asterisk are the values we have obtained to give a reasonable fit to the data. The last column lists the values obtained in previous analyses (Refs. 4 and 5). The numbers in square brackets indicate reference numbers.

Nucleus	E_x (MeV)		$B(E\lambda)$ (e^2b^{λ})		$\frac{(\beta R)_C}{\sqrt{4\pi}}$ (fm)	$\frac{(\beta R)_N}{\sqrt{4\pi}}$ (fm)		Same from Refs. 4 and 5
^{16}O	2^+	6.92	0.0038	[12]	0.300	0.268	[13]	
	3^-	6.13	0.0014	[12]	0.608	0.398	[13]	
^{58}Ni	2^+	1.45	0.0674	[14]	0.236	0.280*		0.264
	3^-	4.47	0.0186	[14]	0.267	0.260		
^{88}Sr	2^+	1.836	0.114	[15]	0.197	0.170*		0.179
	3^-	2.734	0.062	[15]	0.272	0.185*		0.179
^{40}Ca	2^+	3.90	0.0092	[16]	0.138	0.125*		0.116
	3^-	3.74	0.0176	[16]	0.465	0.315*		0.305
	5^-	4.49	2.7×10^{-4}	[5]	0.344	0.175*		0.152
^{48}Ca	2^+	3.832	0.0086	[17]	0.126	0.190*		0.175
	3^-	4.505	0.0065	[17]	0.250	0.190*		0.189
	5^-	5.146	9.1×10^{-6}	[5]	0.049	0.038*		0.064

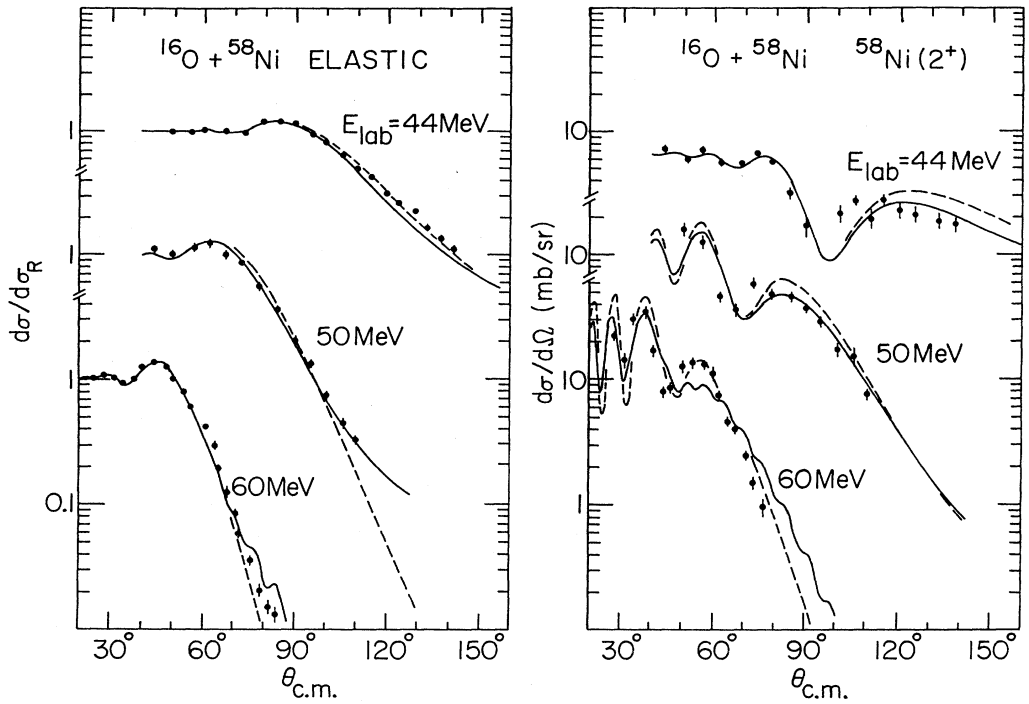

FIG. 1. Angular distributions for elastic scattering of ^{16}O on ^{58}Ni and for the inelastic excitation of the 2^+ state at 1.45 MeV in ^{58}Ni, at three different bombarding energies. The results of calculations which include the coupling to the low-lying 2^+ state in ^{58}Ni, are shown as dashed curves, whereas the fully drawn curves were obtained by also including the 3^- state and the 2^+ and 3^- states of ^{16}O given in Table I. The data are from Ref. 4.

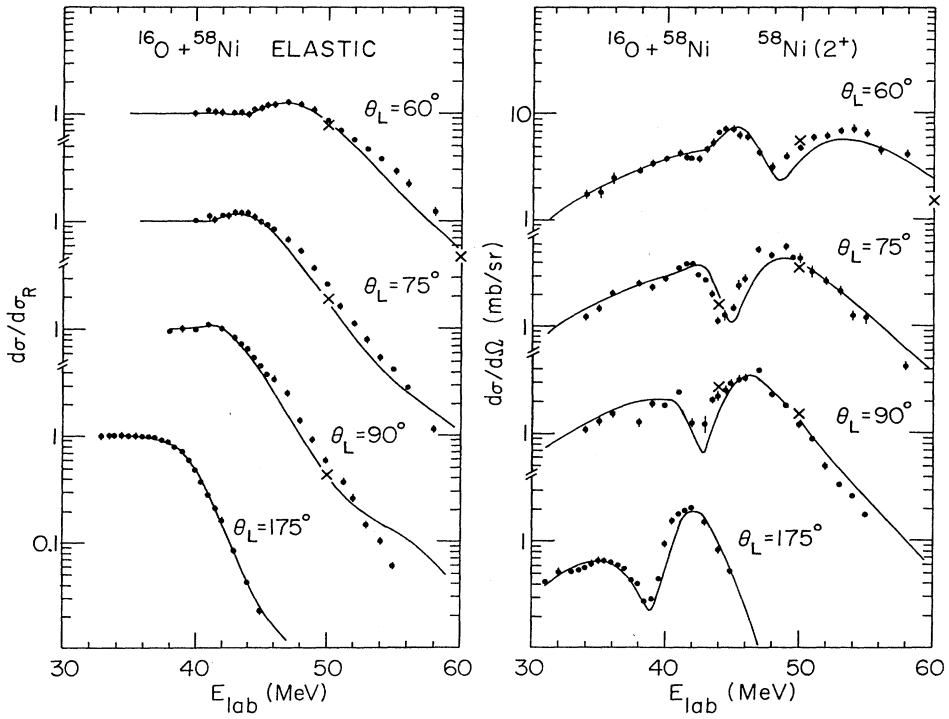

FIG. 1. Angular distributions for elastic scattering of ^{16}O on ^{58}Ni and for the inelastic excitation of the 2^+ state at 1.45 MeV in ^{58}Ni, at three different bombarding energies. The results of calculations which include the coupling to the low-lying 2^+ state in ^{58}Ni, are shown as dashed curves, whereas the fully drawn curves were obtained by also including the 3^- state and the 2^+ and 3^- states of ^{16}O given in Table I. The data are from Ref. 4.

Fig. 2. The interpolated values, indicated by crosses, are about 20–25 % lower than the data obtained in the fixed angle measurements. An evaluation of the original data gives systematic errors of about 10% due to beam energy, angular positions, and target thicknesses, both for the angular distributions and the excitation functions. The different data sets are thus not inconsistent. Disagreements between calculations and experimental data at the 10% level, when making a global comparison, should not be considered as a discrepancy. Finally, the calculated cross sections at the 1% level of Rutherford scattering are higher than the data. This may reflect a lack of absorption due to other channels, as, for example, nucleon transfer, which is expected to become more important with increasing beam energy.

The energy dependence of the measured inelastic 2^+ cross sections shown in Fig. 2 is reproduced very well by the calculations. The overall agreement is in fact better than obtained in the optical-model calculations performed in Ref. 4, which allowed for a Woods-Saxon shaped, energy-dependent optical potential.

We have performed similar calculations for the $^{16}O+^{88}Sr$ scattering. A comparison to the data is shown in Fig. 3. Note the good agreement, both with the 2^+ and the 3^- excitation. The general trend is very similar to the $^{16}O+^{58}Ni$ scattering, and we shall therefore not discuss them here in further detail.

Let us finally mention that the nuclear coupling strengths given in Table I agree to better than 10% with the values extracted from the optical-model analysis performed in Ref. 4. This may seem surprising, at first sight, since the parameters for the ion-ion potential are quite different in the two approaches. They produce, however, almost identical barrier heights and the nuclear form factors are very similar in the barrier region.

IV. $^{16}O+^{40}Ca$ AND $^{16}O+^{48}Ca$ SCATTERING

We have also applied our method to the scattering of ^{16}O on ^{40}Ca at 60 MeV and on ^{48}Ca at 56 MeV. To obtain a satisfactory agreement with the ^{40}Ca data, in particular for the weak excitation of the 5^- state, it was necessary in the original analysis[5] to use coupled-channels calculations, which include the low-lying states in ^{40}Ca. The most dominant coupling effect was due to the inelastic excitation of the strong, collective 3^- state. The calculations performed in Ref. 5 also employed an adjustable imaginary potential.

The results of our calculations are shown in Fig. 4. The fully drawn curves are the results we obtain when we

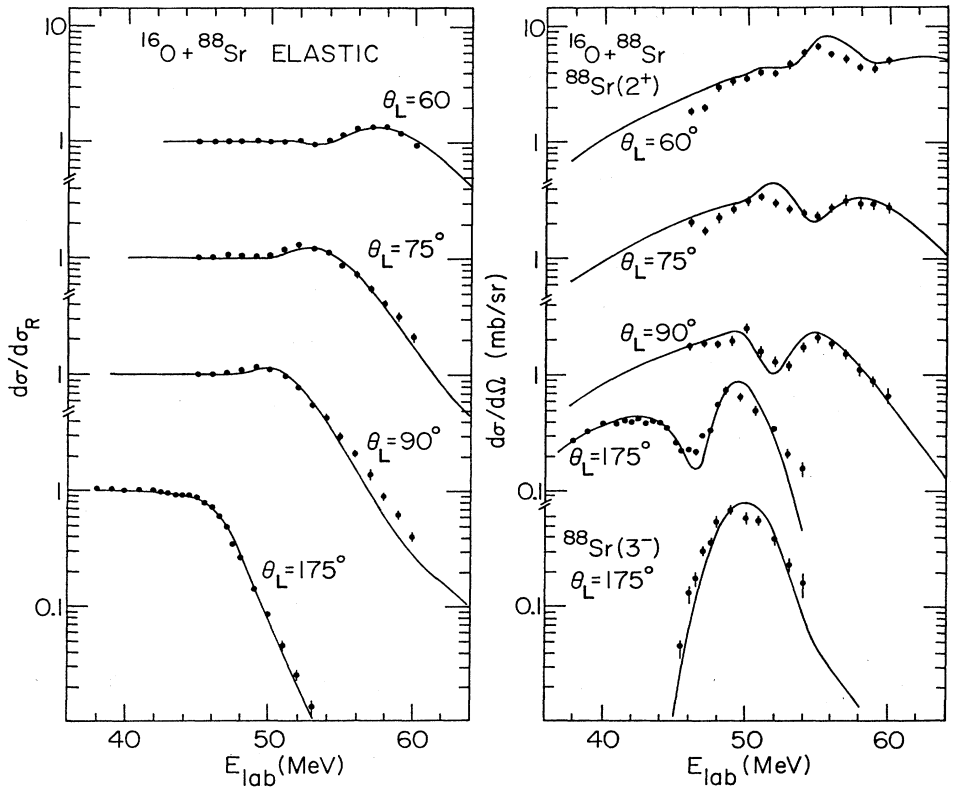

FIG. 3. Energy dependence of the differential cross section for elastic scattering of ^{16}O on ^{88}Sr and for the inelastic excitation of the 2^+ state at 1.836 MeV in ^{88}Sr, at four different scattering angles. Also shown are the cross sections for the excitation of the 3^- state at 2.73 MeV in ^{88}Sr at 175° scattering. The curves show the results of coupled-channels calculations which include all the states given in Table I, for both projectile and target. The data are from Ref. 4.

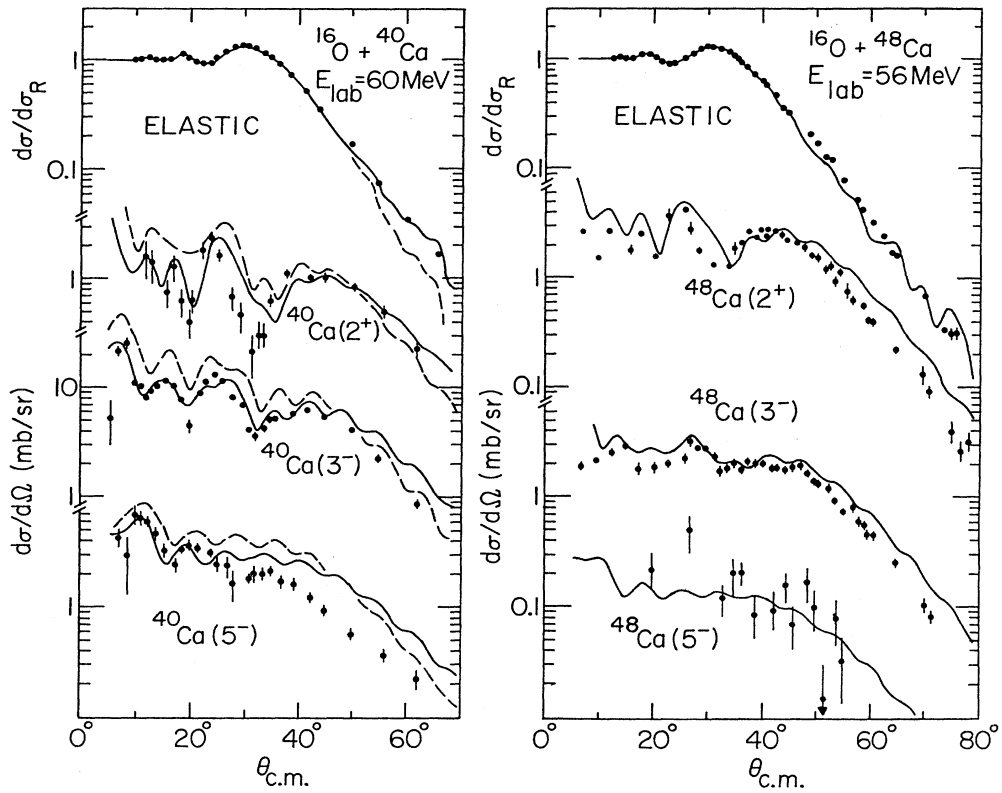

FIG. 4. Angular distributions for elastic and inelastic scattering of ^{16}O on ^{40}Ca at 60 MeV, and on ^{48}Ca at 56 MeV. The fully drawn curves were obtained by including all the states given in Table I, for both projectile and target. The dashed curves are the results we obtain when we only include the low-lying 2^+, 3^-, and 5^- states in ^{40}Ca. The data are from Ref. 5.

include all the states given in Table I, for both projectile and target. The nuclear coupling strengths were adjusted to fit the data at forward angles. The dashed curves are the results we obtained for $^{16}O+^{40}Ca$ when we only include the ^{40}Ca states in the coupled equations. The effect of the ^{16}O states is seen to be significant. One can obtain a better agreement with the inelastic data in the calculations that only include the ^{40}Ca states by reducing the nuclear coupling strengths by about 15%. The effect of the ^{16}O states is larger than in the $^{16}O+^{58}Ni$ scattering. This is due to the fact that the cross sections are more sensitive to nuclear couplings, since the ratio of nuclear to Coulomb form factors is larger in the lighter scattering system.

The agreement with the data is almost as good as obtained in Ref. 5. The major difference between the two calculations is the presence of oscillations at large scattering angles in our calculated angular distributions for elastic scattering. The calculations performed in Ref. 5 included an imaginary potential, and the angular distributions for the elastic scattering are much smoother. It is, however, very satisfying that we are able to reproduce the main features of the data so well in a coupled-channels treatment, using a real, energy-independent ion-ion potential. In fact, the only parameters we have adjusted in order to fit the data are the nuclear coupling strengths, whereas the modification of the radius parameter for ^{40}Ca discussed in Sec. II can be predicted from the measured rms radii of the calcium isotopes.

The quality of the fits shown in Fig. 4 are similar for the two different scattering systems. The remaining discrepancies may be reduced by including more couplings. One example is four-particle transfer, which is the most dominant transfer channel for $^{16}O+^{40}Ca$ and it has a similar strength for $^{16}O+^{48}Ca$.[18] Another example is one-nucleon transfer which is much smaller for $^{16}O+^{40}Ca$ than for $^{16}O+^{48}Ca$, where it has a magnitude that is close to the inelastic cross section.[18] It would be very instructive to perform coupled-channels calculations which also include the most dominant transfer channels for these two systems in order to assess their effect on elastic and inelastic scattering more explicitly.

V. CONCLUSIONS

We have performed coupled-channels calculations for the elastic and inelastic scattering of ^{16}O on a variety of targets including the low-lying states of both projectile and target. Fusion is simulated by ingoing wave boundary conditions in all channels at a distance located inside the Coulomb barrier. One- and two-nucleon transfers are suppressed for most of the systems we have considered at energies near the Coulomb barrier, and we have neglected them in the calculations. The overall agreement with

systematic measurements of the elastic scattering and the 2^+ excitation of the target is qualitatively as good as obtained in previous DWBA analyses. The 2^+ and 3^- states in ^{16}O have a significant influence on the calculated cross sections. Some discrepancies appear, in particular at the higher beam energies and large scattering angles, which may indicate a lack of absorption due to neglected reaction channels.

A coupled-channels treatment, which includes the most dominant reaction channels, seems feasible for many scattering systems at energies near the Coulomb barrier. It is also a more attractive approach than conventional DWBA calculations, since one can study the interplay between the different reaction channels and obtain a consistent description. The input is strongly constrained, either by an empirically determined ion-ion potential or folding potentials and form factors, whereas the energy-dependent polarization potentials are generated by the explicit couplings. An obvious extension of our calculations is to study reactions, where transfer is important, and in particular to study the effect of higher-order couplings such as, for example, the transfer coupling between excited states.

ACKNOWLEDGMENTS

We are grateful to S. Landowne and K. E. Rehm for comments and discussions. This work is supported by the U.S. Department of Energy, Nuclear Physics Division, under Contract W-31-109-ENG-38.

[1]J. S. Lilley, B. R. Fulton, M. A. Nagarajan, I. J. Thompson, and D. W. Barnes, Phys. Lett. **151B**, 181 (1985).
[2]B. R. Fulton, D. W. Barnes, J. S. Lilley, M. A. Nagarajan, and I. J. Thompson, Phys. Lett. **162B**, 55 (1985).
[3]M. A. Nagarajan, C. Mahaux, and G. R. Satchler, Phys. Rev. Lett. **54**, 1136 (1985).
[4]P. R. Christensen, I. Chernov, E. E. Gross, R. Stokstad, and F. Videbaek, Nucl. Phys. **A207**, 433 (1973).
[5]K. E. Rehm, W. Henning, J. R. Erskine, and D. G. Kovar, Phys. Rev. Lett. **40**, 1479 (1978); Phys. Rev. C **25**, 1915 (1982); see also R. J. Ascuitto, J. F. Petersen, and E. A. Seglie, Phys. Rev. Lett. **41**, 1159 (1978).
[6]P. R. Christensen and A. Winther, Phys. Lett. **65B**, 19 (1976).
[7]P. R. Christensen, V. I. Manko, F. D. Becchetti, and R. J. Nickles, Nucl. Phys. **A207**, 33 (1973); R. L. Robinson, H. J. Kim, and J. L. C. Ford, Jr., Phys. Rev. C **9**, 1402 (1974).
[8]N. Anantaraman, Phys. Rev. C **8**, 2245 (1973).
[9]I. J. Thompson, M. A. Nagarajan, J. S. Lilley, and B. R. Fulton, Phys. Lett. **157B**, 250 (1985).
[10]S. C. Pieper, M. J. Rhoades-Brown, and S. Landowne, Phys. Lett. **162B**, 43 (1985).
[11]G. D. Alkhazov, T. Bauer, R. Bertini, L. Bimbot, O. Bing, A. Boudard, G. Bruge, H. Catz, A. Chaumeaux, P. Couvert, J. M. Fontaine, F. Hibou, G. J. Igo, J. C. Lugol, and M. Matoba, Nucl. Phys. **A280**, 365 (1977).
[12]F. Ajzenberg-Selove, Nucl. Phys. **A460**, 1 (1986).
[13]K. T. Knöpfle, G. J. Wagner, H. Breuer, M. Rogge, and C. Mayer-Böricke, Phys. Rev. Lett. **35**, 779 (1975).
[14]L. K. Perker, Nucl. Data Sheets **42**, 457 (1984).
[15]R. L. Bunting and J. J. Kraushaar, Nucl. Data Sheets **18**, (1976).
[16]P. M. Endt and C. Van Der Leun, Nucl. Phys. **A310**, 548 (1978).
[17]D. E. Alburger, Nucl. Data Sheets **45**, 607 (1985).
[18]S. E. Vigdor, in Proceedings of the Symposium on Macroscopic Features of Heavy-Ion Collisions, Argonne, 1976, Argonne National Laboratory Report ANL/PHY-76-2, 1976, p. 95; see also D. G. Kovar, W. Henning, B. Zeidman, Y. Eisen, J. R. Erskine, H. T. Fortune, T. R. Ophel, P. Sperr, and S. E. Vigdor, Phys. Rev. C **17**, 83 (1978).